Nonequilibrium Hypersonic Flows over Corners

Maurizio Pandolfi,* Renzo Arina,† and Nicola Botta†
Politecnico di Torino, Torino, Italy

The hypersonic nonequilibrium flow of air over concave and convex corners is investigated. The description of the flowfield is based on the Euler equations and a chemical model that accounts for the finite rate reactions. An upwind formulation and the related space-marching technique are developed in order to achieve the numerical solution of the fluid dynamical and chemical equations, coupled together. The attention is focused on the effects of nonequilibrium chemistry on fluid dynamics. The transition from the frozen flow condition, just behind the corner, and the equilibrium flow, reached at very large distances far downstream, is characterized by intermediate strong nonequilibrium chemical processes. Such a transition promotes dissipations that, in turn, generate vorticity.

I. Introduction

THE physics of hypersonic flows is complex and intricate. Some aspects are described by the Euler equations, others are related to viscosity and thermal conductivity, as accounted by the additional terms of the Navier-Stokes equations. In addition, there are real gas effects due to the chemical reactions triggered by the high temperature regime. In this paper, we focus our attention on some nonequilibrium effects, namely, on the dissipation generated by the finite rate reactions. In order to emphasize these effects, we can restrict the description of the phenomenology to the Euler equations for a chemically evolving gas (air in particular) and neglect viscosity and thermal conductivity.

The problem we investigate is the two-dimensional flow over a corner either concave (as a wedge) or convex (as in the classical Prandtl-Meyer expansion). Even if such geometries are quite simple, the analysis will contribute to the understanding of some rather complex phenomena that occur in practical problems, such as the front region (inlet) and the rear one (external nozzle) of propulsion devices (scramjet) for hypersonic transports.

Since we consider steady-state configurations, we drop the time derivatives in the Euler equations. Assuming that the velocity regime is supersonic everywhere, these equations present a hyperbolic character with reference to any streamline-like space coordinate in the physical domain.

The chemical description of the air is based on a model widely quoted in the literature.[1] Five species (O, N, NO, O_2, N_2) and 17 reactions are considered. The vibrational energy is assumed to correspond to a half-excited mode. Such a hypothesis can be considered appropriate for applications concerning the aerothermodynamics of re-entry vehicles.[1] The assumption of the full excited mode, or the more sophisticated one of the equilibrium values for the vibrational energy, would imply only slight quantitative variations of the final numerical results. No ionization is considered; the nonequilibrium of the air is purely chemical. We note that the essentials of the present investigation are not related specifically to the assumed chemical model.

Since we neglect diffusion of the species, equations can be written along streamlines that lead to the prediction of the concentrations only on the basis of rates of the reactions provided by the chemical model. These equations present the same hyperbolic nature as the previous ones that describe the fluid dynamics.

The Euler and chemical equations are strongly coupled. The first ones control the pressure (and related temperature) as due to the fluid dynamics. These values strongly affect the rate of production of the species. On the other hand, any variation in species concentration leads to remarkable changes in temperature because of the high formation energies. This fact is reflected back in the fluid dynamics. A parameter that determines the degree of the stiffness of this coupling is the Damköhler number, the ratio between a reference fluid dynamical length and a reference chemical length. High values of this number denote flow configurations close to local equilibrium. Low values refer to almost frozen conditions. In both of the extreme cases, there is no dissipation related to the chemical effects. In the intermediate range of the Damköhler number, we expect a typical nonequilibrium phenomenon and the occuring of the related dissipation.

In the following we discuss a proper arrangement of the Euler equations for the steady state, according to the upwind *lambda* formulation.[2] Since both sets of equations are hyperbolic, we can use the space-marching technique (integration along a proper space coordinate) to predict the evolution of the flowfield downstream of the corner. A proper one-sided finite difference approximation is used in the numerical scheme. We then show how the oblique shock is treated in the wedge problem. It is fitted as a discontinuity with jump conditions corresponding to *generalized nonequilibrium* Rankine-Hugoniot (RH) relationships. At this point we analyze the physics of these problems. Finally, we comment on our numerical results.

II. Equations

We consider the Euler equations for the two-dimensional problem and for the steady-state configuration:

$$V \cdot \nabla \rho + \rho \nabla \cdot V = 0 \tag{1a}$$

$$(V \cdot \nabla) V + (\nabla p / \rho) = 0 \tag{1b}$$

$$V \cdot [\nabla h - (\nabla p / \rho)] = 0 \tag{1c}$$

Here, V, ρ, p, and h denote the velocity vector, density, pressure, and enthalpy, respectively.

Following Ref. 1, we neglect the diffusion of the species and we write the equations of the production of the species along streamlines:

$$V \cdot \nabla q_i = \omega_i, \qquad i = 1,2,3 \tag{2}$$

Received Feb. 21, 1989; revision received Nov. 17, 1989; accepted for publication Jan. 4, 1990.

*Professor, Department of Aeronautical and Space Engineering. Associate Fellow AIAA.

†Research Scientist, Department of Aeronautical and Space Engineering.

where the index i refers to O, N, and NO, respectively. The concentration ($g - mole \cdot g^{-1}$) is denoted by q_i, and the source term ω_i gives the rate of production for each species. The mass conservation law provides the concentration q_4 and q_5 of O_2 and N_2, respectively:

$$q_4 = \frac{0.21}{\mu} - \frac{q_1 + q_3}{2}; \qquad q_5 = \frac{0.79}{\mu} - \frac{q_2 + q_3}{2}$$

where μ is the average molecular weight of the air. Formulas and constants for computing ω_i are given fully in Ref. 1.

The equation of state is

$$p = \rho R T \mathcal{Z}$$

where T is the temperature and $\mathcal{Z}$ the compressibility factor, which is defined as

$$\mathcal{Z} = 1 + \mu \frac{q_1 + q_2}{2}$$

The enthalpy is given by

$$h = \frac{p}{\rho}\frac{3 + \mathcal{Z}}{\mathcal{Z}} + \sum_{i=1}^{3} h_i^0 q_i \tag{3}$$

where h_i^0 are the formation energies of the species O, N, and NO.

By differentiating Eq. (3) and by using the energy equation [Eq. (1c)] and Eq. (2), we obtain

$$V \cdot \nabla \rho = (1/a^2) V \cdot \nabla p - \Psi \tag{4}$$

Here, a defines the frozen speed of sound:

$$a^2 = \frac{\partial h}{\partial \rho}\Big/\left(\frac{1}{\rho} - \frac{\partial h}{\partial p}\right)$$

and Ψ the contribution of the source terms in Eq. (2):

$$\Psi = \sum_{i=1}^{3} \left(\omega_i \frac{\partial h}{\partial \rho}\right)\Big/\frac{\partial h}{\partial p}$$

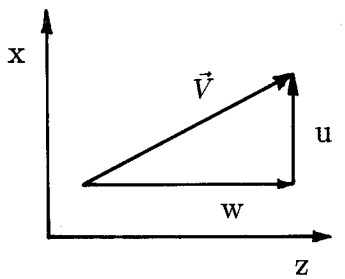

Fig. 1 Coordinates and velocity components.

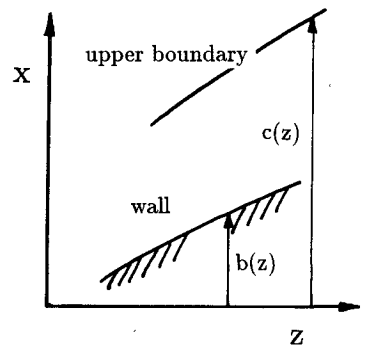

Fig. 2 Definition of the boundaries.

By using Eq. (4), the Euler equations [Eqs. (1a-c)] are written in terms of (p, h, V) as dependent variables. Then it is convenient to introduce the slope of a streamline (Fig. 1), where u and w are the velocity components

$$\sigma = u/w$$

since this represents a significant variable in supersonic flows. The Euler and the chemical equations then become

$$[1 - (a^2/w^2)]p_z + \sigma p_x + \rho a^2 \sigma_x = (a^2/w)\Psi \tag{5a}$$

$$\sigma_z + \sigma\sigma_x + [(p_x - \sigma p_z)/\rho w^2] = 0 \tag{5b}$$

$$h_z - (p_z/\rho) + \sigma[h_x - (p_x/\rho)] = 0 \tag{5c}$$

$$(q_i)_z + \sigma(q_i)_x = \omega_i/w, \qquad i = 1,2,3 \tag{5d}$$

It is now convenient to introduce a computational frame (X, Z) defined as

$$X = \frac{x - b(z)}{c(z) - b(z)}, \qquad Z = z$$

As shown in Fig. 2, the computational region appears confined by the two boundaries $b(z)$ and $c(z)$. The first, $b(z)$, determines the geometry of the wall. The second, $c(z)$, refers to the location of the fitted oblique shock for the concave angle corner, or of the first characteristic of the expansion fan for the convex angle case. Eqs. (5a-d) can be written with reference to the new independent variables (X,Z).

The attention is now focused on the hyperbolic nature of the problem. Since we expect the velocity supersonic component along z, this will be assumed as the hyperbolic (or time-like) coordinate. Proper arrangement of Eqs. (5a-c) provides compatibility equations that describe the convection of signals along characteristic lines. This step follows the classical upwind lambda formulation.[2] We note that Eq. (5d) is written already in a convection form and does not need any further arrangement. The final form of these convection equations is the following:

$$(U_j)_z + \Lambda_j (U_j)_x = R_j, \qquad j = 1,\ldots,6 \tag{6}$$

The signals are defined as differentials:

$$dU = \begin{bmatrix} dp - \rho w^2/\beta \cdot d\sigma \\ dh - dp/\rho \\ dp + \rho w^2/\beta \cdot d\sigma \\ dq_1 \\ dq_2 \\ dq_3 \end{bmatrix}$$

where

$$\beta = \sqrt{(u^2 + w^2)/a^2 - 1}$$

The slope of the characteristic lines, along which the signals are convected, are defined as

$$\Lambda = \begin{bmatrix} X_z + X_x(w^2\sigma - a^2\beta)/(w^2 - a^2) \\ X_z + X_x\sigma \\ X_z + X_x(w^2\sigma + a^2\beta)/(w^2 - a^2) \\ X_z + X_x\sigma \\ X_z + X_x\sigma \\ X_z + X_x\sigma \end{bmatrix}$$

The source terms, all related to the chemical kinetics, are

$$R = \begin{bmatrix} \Psi a^2 w(\beta - \sigma)/[\beta(w^2 - a^2)] \\ 0 \\ \Psi a^2 w(\beta + \sigma)/[\beta(w^2 - a^2)] \\ \omega_1/w \\ \omega_2/w \\ \omega_3/w \end{bmatrix}$$

III. Numerical Procedure

The system of Eqs. (6) is integrated according to the space-marching technique along the coordinate Z. In fact, from Eq. (6), for $j = 1,2,3$, we obtain three equations with the unknowns $(p)_z$, $(\sigma)_z$, and $(h)_z$. These and Eq. (6), for $j = 4,5,6$, will be integrated numerically. The X derivatives are approximated by *upwind* finite differences. The sign of Λ_j defines the side on which to evaluate the one-sided finite difference approximation for $(U_j)_x$. Since we integrate the equations of the fluid dynamics and chemistry fully coupled, we expect possible numerical problems due to the stiffness between the two sets of equations at high Damköhler numbers.

To overcome them, we adopt a semi-implicit algorithm for the chemical equations [Eq. (6), for $j = 4,5$, and 6], a standard procedure in these cases. Namely, the values of the source terms (ω_i) during each integration step are evaluated on the basis of the initial data of the thermodynamical properties and on both initial and final values of the concentrations. The X derivatives of the concentrations, $(q_i)_x$, are evaluated only from the initial data. The integration of the fluid dynamical equations [Eq. 6), $j = 1,2$ and 3] is carried out explicitely and retains the values ω_i just computed with the semi-implicit integration of the species needed for the evaluation of the term Ψ that appears in the source terms R_1 and R_3.

The treatment of the oblique bow shock, expected in the wedge problem, is carried out according to the *shock-fitting* technique. The classical RH relationships dictate the jump conditions. They express the classical conservation laws, which retain the concentrations of the species just behind the shock, frozen at the upstream levels ($q_1 = q_2 = q_3 = 0$). Only after the gas has crossed the shock, the high temperature triggers the chemical relaxation that develops smoothly over the shock layer (that is defined as the region bounded by the bow shock and the wall). The width of the nonequilibrium region located behind the shock, over which a particle reaches an equilibrium state, depends on the upstream conditions and the slope of the shock. Such a region will be denoted as the chemical layer. Close to the corner, the chemical layer is larger than the shock layer, or at least of the same order of magnitude as the shock layer. Since the length of a computational interval is the width of the shock layer divided in a finite number of computational intervals, the chemical evolution is spread over a reasonably high number of computational points. Therefore, we do not expect any problem in describing the chemical relaxation numerically. However, far downstream, the shock layer and the size of an interval become very large, whereas the width of the chemical layer remains unchanged. The latter thus becomes a small fraction of the shock layer. In these conditions, the chemical layer is spread over only a few computational intervals. Farther downstream, it is totally swallowed within one interval. Therefore, the numerical prediction of the chemical layer, at least in part, cannot be accomplished because of lack of resolution in the finite approximation of Eq. (6), for $j = 4,5$ and 6.

To overcome this difficulty, we have introduced generalized RH conditions.[3] They represent the conservation laws with finite values of the concentrations (q_1, q_2, q_3) of the new species (O, N, NO) on the high-pressure side. These values account for the chemical evolution that occurs along a streamline that leaves the shock, over the distance that corresponds to the physical extension of a computational interval. In other words, we have made the approximation of including in the jump conditions of the discontinuity the classical conservation laws and a fraction of the chemical layer that would be unpredictable by Eq. (6), for $j = 4,5$, and 6. At a very large distance far downstream of the corner, where the chemical layer is totally hidden in the last interval after the shock, the generalized RH relationships provide the conservation laws that correspond to the full local equilibrium conditions.

The values of the concentrations, needed to evaluate the generalized RH jump conditions, are generated once and for all at the beginning of the computation on the basis of the steady one-dimensional model and then stored on a numerical table for a set of different Mach numbers normal to the shock. Such a numerical device already has been experimented for computing blunt body flows, predicted through a time-dependent technique.[3] A large number of numerical experiments have been carried out. In particular, the effect of the mesh size behind a shock, treated with the classical RH jump conditions, has been investigated. It has been found that, when the mesh is too rough, that is, one grid extends for an appreciable amount of the physical thickness of the chemical layer, the lack of accuracy behind the shock deteriorates, as shown by the loss of conservation of basic properties such as mass flow and total enthalpy.

We point out that this approximation tends to the correct treatment of the shock, followed by the chemical layer, once the number of the computational points is sufficiently increased and the physical extension of the interval tends to a sufficiently small length.

IV. Flow About a Concave Corner

The nonequilibrium hypersonic flow about a concave corner was investigated many years ago. A review of results available at that time is reported in Ref. 4. Here, we resume that analysis and aim to contribute to the understanding of the problem. The description of this flowfield is simple under the assumption that the physics is described by the Euler equations only, without any chemical effect. The oblique shock wave separates the upstream uniform region from a second uniform region that extends over the wedge. The slope of the shock is such that the deflection of particles through the shock itself brings the streamlines all parallel to the wall of the wedge. Such a deflection is achieved with a sudden reduction of the component of the velocity normal to the shock (RH conditions) and by leaving the parallel component unchanged.

This picture is valid also for the chemically reacting flow in a very small neighborhood of the corner. Here, the residence time of the particle is extremely small as compared with the reference chemical time (Damköhler number very low). Not enough time is allowed to the concentrations of the species for changing, and their values remain frozen at the upstream levels. Only farther downstream of the corner we begin to observe the development of the chemical relaxation.

The high temperature, generated across the shock and predictable after the laws of conservation with frozen concentrations (classical RH conditions), promotes the dissociation of the original molecules (O_2, N_2). The rates of production of the new species (O, N, NO) are rather high, immediately behind the shock because the temperature is high (a factor that accelerates any chemical event) and the departure from the equilibrium state is the largest. Therefore, the gas behind the discontinuity of the shock begins to dissociate at a very high rate. Nevertheless, these effects become noticeable only at a finite distance behind the shock because the rates of the chemical reactions are high, but finite.

The sequence of the chemical reactions is not very complicated. The dissociation first of O_2 and then of N_2 generates mainly O and N, and also a moderate amount of NO. The latter dissociates farther downstream. The chemical relaxation

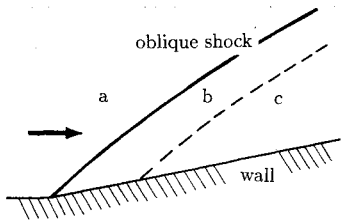

Fig. 3 Flow about a concave corner (wedge).

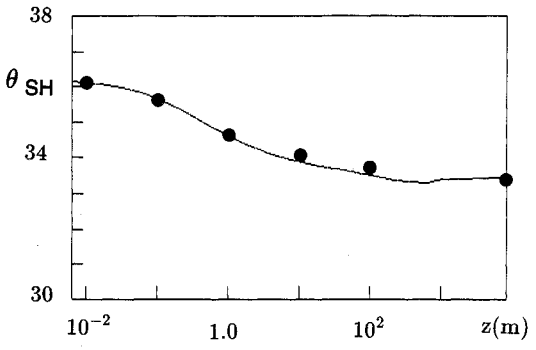

Fig. 4 Shock angle in nonequilibrium flow over a 30-deg wedge: symbols are from Ref. 1 and the solid line refers to the present computations.

toward the equilibrium tends to absorb heat and the temperature decreases. The cooling shrinks the gas and the pressure decreases as we proceed along the wedge. Meanwhile, the oblique shock is pulled and bends downwards.

The weakening of the oblique shock also can be interpreted in terms of the deflection of the streamlines required by the boundary condition (velocity parallel to the wall). As seen earlier, such a deflection is obtained in the whole Eulerian flow (without any chemistry) by the reduction at the shock of the component of the velocity normal to it, whereas the parallel component remains unchanged. This is also the picture we expect in the close proximity of the corner because the particles crossing the shock have no time to go through chemical relaxation: the wall is just below the shock and the particles behave according to the Eulerian mode. However, at a large distance downstream, the shock is not so close to the wall anymore. Thus, time is left to the particles leaving the shock to evolve chemically, before they approach the wall. The development of the dissociation slows down the velocity component normal to the shock, without any alteration of the parallel component. The resulting whole deflection would be larger than the value required by the wall. Therefore, the slope of the shock has to be readjusted and decreases. The correct deflection dictated by the boundary condition at the body will be obtained partly across the weaker oblique shock wave and partly with a smooth evolution over the chemical layer, located just behind the shock.

A qualitative picture of such a flowfield, borrowed from Ref. 1, is shown in Fig. 3. We may distinguish three regions, instead of the two uniform ones of the pure Eulerian flow. First, the upstream uniform region a that terminates at the oblique shock. The intensity of the shock is higher at the corner and weaker when we move downstream. Behind the shock, we note a nonuniform region b. Here, the chemical reactions occur. This region is shaped as a strip, with almost constant width, because the path required by a particle to reach the equilibrium state after the shock transition is practically the same, either close to or far from the corner. Behind the nonequilibrium region the third region, c, extends, Here, all particles have reached their state of equilibrium. However, we can distinguish different conditions of equilibrium. Let us consider a streamline close to the wall. A particle moving on it has crossed the shock on its front part and has undergone a certain dissipation. On the contrary, another particle moving on a streamline located well above the wall has crossed a weaker shock farther downstream. This particle has undergone a smaller dissipation. After the shock, further dissipation is generated on the two particles through region b, due to the nonequilibrium. Once these two particles have exhausted their chemical relaxation and move downstream throughout region c, they reach a uniform pressure because all the streamlines flow parallel to the wall. Because of the different dissipations, the equilibrium conditions for the two particles are different. We emphasize that two factors contribute to the dissipation: the shock and the nonequilibrium relaxation.

Such a difference is also revealed by the lower velocity near the wall, where we find those particles that have undergone a larger dissipation. The velocity gradient normal to the wall shows the presence of vorticity, consistent with the different levels of dissipation. Finally, we note that the defect of velocity near the wall corresponds to higher static temperature, which implies also a more relevant degree of dissociation.

We have performed some computations on this problem. The initial data are taken from Ref. 1. We consider a 30-deg wedge. The upstream conditions are Mach number $M_\infty = 21.7$, pressure $p_\infty = 10.85(\mathrm{N/m^2})$, and temperature $T_\infty = 237.1(K)$. They correspond to the speed of 6.7(km/s) at the altitude of 65.5(km). The variation of the angle of the shock θ_{sh} is shown in Fig. 4. Here, and in the following figure, the logarithm of the coordinate z, with $z = 0$ at the corner, is the abscissa. This representation provides an enlargement of the region close to the corner where most of the phenomenon is taking place. The angle θ_{sh} varies from the value corresponding to the frozen flow configuration down to the value of the full equilibrium flow. A slight undershoot is noticeable. The variation of θ_{sh} may look small, about 3 deg. Nevertheless, it is far from being negligible considering that the angle between shock and wall, at a large distance from the corner, is only 50% of its initial value. The evolution of the pressure at the wall is reported in Fig. 5. We point out the decrease of the pressure from the frozen level at the corner just behind the shock ($p/p_\infty = 187$) to the equilibrium value far downstream ($p/p_\infty = 175$).

It is worthwhile to note that the computation has been continued until a very large distance z without finding

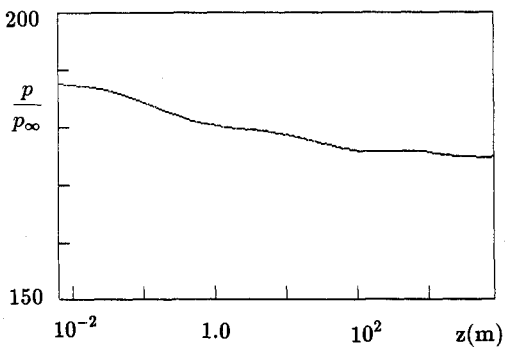

Fig. 5 Pressure at the wall in nonequilibrium flow (30-deg wedge).

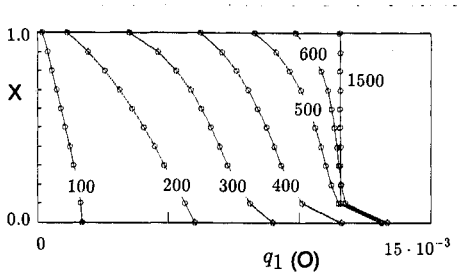

Fig. 6 Concentration of q_1 (atomic oxygen) over the shock layer (30-deg wedge).

numerical difficulties related to the lack of resolution behind the shock, as reported in Ref. 1. This has been made possible by the definition of the previously mentioned generalized RH relationships. At the largest value of z, the configuration of complete chemical equilibrium (slope of the shock included) has been reached and no further changes have been noticed in the numerical outputs.

It is interesting to follow the nonequilibrium evolution along the ramp. We have reported the development of the concentration of O and NO in Figs. 6 and 7. The ordinate is the normalized coordinate X ($X = 0$ at the wall and $X = 1$ at the shock) and the concentrations are reported on the abscissa; K is the number of integration steps. At $K = 100$, which corresponds to a station quite close to the corner [$z = 5.4 \cdot 10^{-2}$(m)], the amount of O is very small and that of NO negligible. Farther downstream, at $K = 200$ [$z = 0.54$(m)], the distribution of the concentration of O over the shock layer is monotonic, the maximum being at the wall. The particles flowing along the wall had a longer time to develop dissociation. On the contrary, we note that the dissociation of O is still very small at the shock; that is, the generalized RH conditions include a negligible part of the chemical relaxation. This means that the grid size is still small with respect to the width of the chemical. layer (complete relaxation distance), and the jump conditions at the shock are close to the classical ones. The concentration of NO shows a similar behavior. At $K = 300$ [$z = 4.38$(m)], the grid size becomes large enough to prevent any reliable description of the chemical processes occuring in the computational interval behind the shock. Therefore, the generalized RH conditions include a large part of the chemical relaxation, as it can be seen by the high concentration of O at the shock. The distribution of NO looks rather interesting. At the wall, the typical maximum value of the NO concentration has already been reached and its dissociation just started. The largest concentration of NO occurs now in the middle of the shock layer. At larger K, the gas that first came through the shock, near the corner, is confined close to the wall ($X = 0$) and covers a diminishing percentage of the physical extension of the shock layer. At $K = 600$ [$z = 666$(m)], the concentration of O begins to reach a uniform value distribution all over the shock layer, except the different value of equilibrium at the wall. The same comments can be made for NO. Much farther downstream, at $K = 1500$ [$z = 8 \cdot 10^3$(m)], the shock layer appears as a uniform flow region. Its quantitative description corresponds to the classical equilibrium flow regime. However, we expect to find two small regions with different properties, one at the shock and one at the wall. At the shock, a chemical layer should follow the shock itself. Since its physical width is much smaller than the amplitude of an interval, it will be included inside the generalized RH conditions. At the wall, the gas that crossed the shock in the front part and experimented the strongest dissipation has now reached a different equilibrium state. Since the pressure is constant througout the shock layer, the velocity at the wall will be lower than in the core of the shock layer. This is shown in Fig. 8, where the distribution of the velocity, at $K = 1500$, over the shock layer has been plotted. The velocity defect at the wall reveals the vorticity generated in the neighborhood of the corner.

These results agree rather well with those presented in Ref. 1. The symbols in Fig. 4 refer to the shock angle as predicted in Ref. 1, the last symbol [at $z = 10^4$(m)] representing the equilibrium value. The agreement is quite good with a slight deviation appearing at $z = 100$(m), where, however, the result from Ref. 1 may be not fully reliable (shock angle fails to converge to the equilibrium value). Also, the comparison for nonequilibrium properties is satisfactory. For instance, the concentration of the atomic oxygen on the wall, at $z = 0.34$, 3.48, and 29.60(m), has been predicted at 0.0052, 0.0086, and 0.0115, whereas the values taken from Ref. 1 are estimated as 0.0059, 0.0091, and 0.0122. The agreement looks good, taking into consideration that these evaluations are very sensitive.

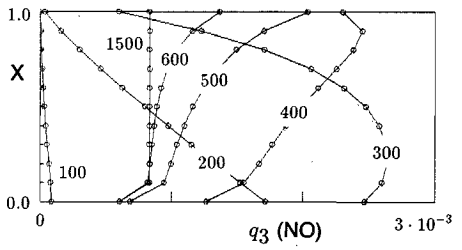

Fig. 7 Concentration of q_3 (nitric oxide) over the shock layer (30-deg wedge).

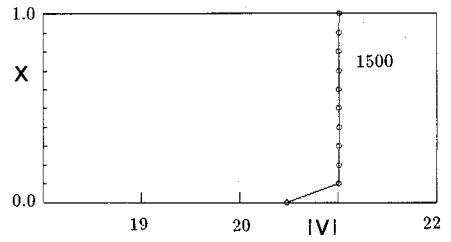

Fig. 8 Distribution of the velocity over the shock layer (30-deg wedge).

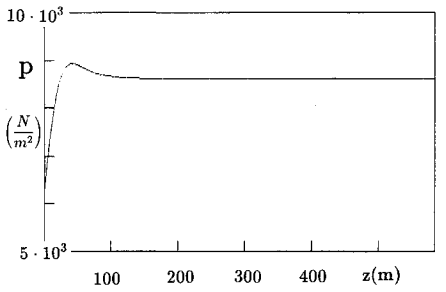

Fig. 9 Pressure at the wall in nonequilibrium flow (10-deg convex corner).

V. Flow About a Convex Corner

This problem is both similar and different with respect to the previous one. It also has been discussed and commented in Ref. 4.

We may begin the analysis by recalling the flow configuration described by the Euler equations in the absence of chemical effects. We know that there are two uniform regions, one upstream and one along the inclined wall, where the flow has been fully deflected. These two regions are separated by a classical Prandtl-Meyer expansion fan that replaces the oblique shock seen in the previous example. Flow properties change smoothly throughout the fan, but assume constant values on each of its ray. In fact, the solution is self-similar because no reference length appears. However, if finite rate chemical reactions are considered, a reference time (or length), related to the nonequilibrium process, is introduced and simplicity is lost.

Let us assume a rather high level of enthalpy in the upstream flow. The concentrations correspond to the equilibrium condition and we expect a remarkable degree of dissociation.

In a very close neighborhood of the corner, the configuration is still represented by the Prandtl-Meyer expansion fan, where the concentrations are frozen to their upstream levels. Such a picture holds for a relevant distance after the corner since the low temperature, due to the sudden expansion at the sharp corner, keeps the reactions rates low. Nevertheless, as soon as the dissociated species tend to recombine, the released heat of formation increases the temperature and the speed of the reactions. We note that in the wedge problem the situation was reversed: the high temperature induced by the shock was damped by the forthcoming dissociation. By proceeding along

the wall, the recombination of the dissociated species leads to a strong increase of the temperature. The phenomenon is similar to the process described by the Rayleigh curve; that is the addition of heat in the one-dimensional flow of perfect gas. The pressure also increases along z.

Far above the wall, the situation is rather different. There, the expansion fan is very large and the pressure decreases smoothly on a streamline, compared with the sudden expansion jump at the corner. With such a slow transition through different pressure levels, enough time is left to the gas to recombine, and the chemical evolution closely resembles a sequence of nearly equilibrium states. At the corner, the Damköhler number tends to zero and, far above, to infinity. Let us consider two particles: one runs close to the wall, the other far above. They reach two distinct states of equilibrium downstream. The former has gone through a strong nonequilibrium transformation and, therefore, has experimented the related high dissipation. The second has followed a sequence of equilibrium states, that is, a reversible transformation, without any dissipation. In the final equilibrium states, both particles share the same pressure, but the velocity is lower at the wall, due to the higher dissipation. Such a shear flow shows a generation of vorticity, strictly related to the variation of dissipation on different streamlines.

We would like to stress the difference in nonequilibrium effects between the flow about a concave corner and the flow about a convex corner. In the former, both shock and nonequilibrium chemical layer contribute to the generation of different levels of dissipation over distinct streamlines. In the latter, nonequilibrium is the only source of dissipation, different on distinct streamlines.

We have performed a few computations to confirm the previous description. For an example, we present results for the case $M_\infty = 4.15$, $p_\infty = 38.1 \cdot 10^3$ (N/m^2), $T_\infty = 5715(K)$ as upstream conditions. In a state of chemical equilibrium, the concentrations are $q_{1\infty} = 1.43 \cdot 10^{-2}$, $q_{2\infty} = 7.87 \cdot 10^{-2}$, and $q_{3\infty} = 2.59 \cdot 10^{-4}$. The molecular oxygen is almost fully dissociated ($q_{4\infty} = 7.0 \cdot 10^{-6}$), whereas the molecular nitrogen is dissociated only moderately ($q_{5\infty} = 2.34 \cdot 10^{-2}$). We have considered the expansion about at 10-deg corner. The evolution of the pressure at the wall ($X = 0$) along z is shown in Fig. 9. Here, the abscissa refers to the coordinate z, not to ($\ell n\, z$) as in previous figures, because the chemical process develops more smoothly along the wall. At the corner, the pressure drops from the upstream value (p_∞) down to the level of 6235 (N/m^2) after the frozen Prandtl-Meyer expansion fan. The following chemical effects tend to increase the pressure toward its final equilibrium value of 8930(N/m^2). We note that the pressure overshoots, a fact not observed in the monotonic decreasing of the pressure in Fig. 5, even if the angle of the shock was slightly undershooting. Similar overshootings are also reported in Ref. 4, even with a simpler model of the gas.

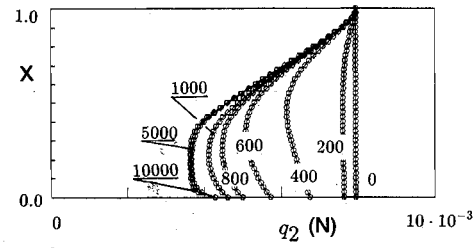

Fig. 10 Concentration of q_2 (atomic nitrogen) (10-deg convex corner).

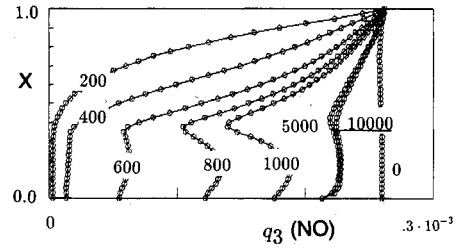

Fig. 11 Concentration of q_3 (nitric oxide) (10-deg convex corner).

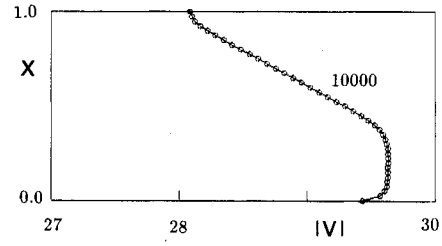

Fig. 12 Distribution of the velocity (10-deg convex corner).

We now focus our attention on the evolution of the chemical species. On the basis of the previous initial data, the atomic oxygen concentration does not change significantly. Therefore, we follow the evolution of the atomic nitrogen and nitric oxide. The distributions of their concentrations over the shock layer, q_2 and q_3, are reported in Figs. 10 and 11. The number K of the integration steps corresponds to relative locations along the wall: $K = 200$ [$z = 0.33$(m)], $K = 400$[$z = 8.64$(m)], $K = 600$[$z = 20.6$(m)], $K = 800$[$z = 32.6$(m)], $K = 1000$[$z = 44.5$(m)], $K = 5000$[$z = 284$(m)], $K = 10{,}000$[$z = 590$(m)]. First we look at Fig. 10. The lower temperature induced by the expansion fan will cut down the concentration of N to an equilibrium value about 50% of the upstream value. The process is relatively slow, compared with the case of a compression corner. At the largest values of K, the distribution is determined all over the flowfield by the local equilibrium conditions reached through a reversible transformation. Close to the wall, however, the dissipation generated in the particles that went through the strong nonequilibrium evolution leads to an equilibrium condition with a higher concentration of N.

We now consider Fig. 11, where the evolution of the concentration of NO is reported. The nitric oxide reacts much faster than the atomic nitrogen to the sudden decrease in temperature. We observe that the concentration at $K = 200$ is totally different from the initial one. A more detailed description, from the initial location at the corner up to $K = 200$, shows that this variation occurs monotonically, just behind the corner. Then, the concentration moves toward the final equilibrium condition, at a speed that is essentially controlled by the rate of reduction of the N concentration. We note that the variations of N and NO, reported in Figs. 10 and 11, do not balance each other (note the different scale in the abscissa) and that almost all of the N that disappears recombines in N_2. The different equilibrium condition at the wall is also evident in the concentration of NO there.

Finally, we note that the effect of the irreversibility and dissipation experimented by the particles flowing near the wall is also denoted, as in the wedge problem, by the profile of the velocity. This is reported in Fig. 12 at $K = 10{,}000$. The smooth variation on the upper part represents the regular expansion fan governed by the local equilibrium conditions. The remnants of the nonequilibrium process developed near the wall, after the frozen expansion at the corner, are confined in the lowest part. The vorticity generated by the nonequilibrium effects is just localized there.

VI. Conclusions

We have investigated the hypersonic flow over corners, both concave and convex. The actual physics has been approximated by the Euler equations and by a nonequilibrium chemical model using 5 species and 17 reactions.

Since we have assumed the flow to be supersonic everywhere, we have rearranged the steady-state Euler equations according to the upwind lambda formulation, conceived for a space-marching technique. The resulting equations express the

evolution of the fluid dynamics as the convection of signals propagating on characteristic lines. The equations that provide the rate of production of the chemical species are already written in convection form. They are characterized by strong source terms, related to the speed of the chemical reactions.

The main feature of the numerical technique used for the prediction of nonequilibrium flows is represented by the definition of the generalized Rankine-Hugoniot relationships that give the jump conditions through the bow shock (for the concave angle corner), suitable for accounting that part of nonequilibrium evolution that occurs over distance as large as the grid intervals. A standard semi-implicit technique is introduced to overcome stiffness problems in near equilibrium conditions.

The numerical method is used as a tool to investigate the nonequilibrium effects induced by a corner deflection on the uniform upstream flow. In the concave angle corner problem, the nonequilibrium process acts on the slope of the bow oblique shock by decreasing its slope from the frozen value at the corner down to the equilibrium flow value far downstream. The variation of the intensity of the shock and the nonequilibrium in the following chemical layer generate different dissipations on distinct streamlines so that vorticity is generated. In the convex angle problem, the sudden expansion at the corner induces strong nonequilibrium on those particles flowing close to the wall; whereas a fully reversible transformation occurs far above the wall, where the expansion goes through a sequence of equilibrium states. The dissipation related to the nonequilibrium leads to the generation of vorticity close to the wall. In addition, a full description of the variation of the chemical species is given. Finally, it can be noted how nonequilibrium processes lead to strong variations of the pressure acting on the wall.

References

[1]Rakich, J. V., Bailey, K. E., and Park, C., "Computation of Non-Equilibrium Three-Dimensional Inviscid Flow over Blunt-Nosed Bodies," *AIAA Journal*, Vol. 21, No. 6, 1983, pp. 834–841.

[2]Moretti, G., "The Lambda-Scheme," *Computers and Fluids*, Vol. 7, No. 3, 1979, pp. 191–205.

[3]Botta, N., Pandolfi, M., and Germano, M., "Non-Equilibrium Reacting Hypersonic Flow About Blunt Bodies: Numerical Prediction," AIAA Paper 88-0514, 1988.

[4]Vincenti, W. G., and Kruger, C. H., *Introduction to Physical Gasdynamics*, Wiley, New York, 1965.